A Refined Analysis on the $X(3872)$ Resonance

Ce Meng,[1, *] Juan José Sanz-Cillero,[2, †] Meng Shi,[3, ‡] De-Liang Yao,[3, 4, §] and Han-Qing Zheng[3, 5, ¶]

[1]*Department of Physics, Peking University, Beijing 100871, China*

[2]*Departamento de Física Teórica and Instituto de Física Teórica,*
IFT-UAM/CSIC Universidad Autónoma de Madrid, Cantoblanco, Madrid, Spain

[3]*Department of Physics and State Key Laboratory of Nuclear Physics*
and Technology, Peking University, Beijing 100871, P.R. China

[4]*Institute for Advanced Simulation, Institut für Kernphysik and Jülich Center for Hadron Physics,*
Forschungszentrum Jülich, D-52425 Jülich, Germany

[5]*Collaborative Innovation Center of Quantum Matter, Beijing, People's Republic of China*

We study the property of the $X(3872)$ meson by analyzing the $B \to KD\bar{D}^*$ and $B \to KJ/\psi\pi^+\pi^-$ decay processes. The competition between the rescattering mediated through a Breit–Wigner resonance and the rescattering generated from a local $D\bar{D}^* \to D\bar{D}^*$ interaction is carefully studied through an effective lagrangian approach. Three different fits are performed: pure Breit-Wigner case, pure $D\bar{D}^*$ molecule case with only local rescattering vertices (generated by the loop chain), and the mixed case. It is found that data supports the picture where X(3872) is mainly a $(\bar{c}c)$ Breit–Wigner resonance with a small contribution to the self–energy generated by $\bar{D}D^*$ final state interaction. For our optimal fit, the pole mass and width are found to be: $M_X = 3871.2 \pm 0.7$MeV and $\Gamma_X = 6.5 \pm 1.2$MeV.

I. INTRODUCTION

The $X(3872)$ is a narrow resonance close to the $D^0\bar{D}^{*0}$ threshold, which was first observed in $B^\pm \to K^\pm J/\psi\pi^+\pi^-$ by the BELLE Collaboration [1], and later confirmed by CDF [2], D0 [3] and BABAR Collaborations [4]. It has also been observed at LHCb [5] and CMS [6]. The new results of Belle show a mass $m_{X(3872)} = 3871.85 \pm 0.27(stat.) \pm 0.19(syst.)$ MeV and width less than 1.2 MeV [7]. A recent angular distribution analysis of the $X \to J/\Psi\pi^+\pi^-$ decay by LHCb has determined the $X(3872)$ quantum numbers to be $J^{PC} = 1^{++}$ [8].

The decay of the X(3872) including $J/\psi\pi^+\pi^-$ and $D^0\bar{D}^{*0}$ and $\bar{D}^0D^{*0}$ final states are studied by BESIII, BABAR and BELLE [9–14]. Furthermore, other $X(3872)$ decay channels that have been observed experimentally are $J/\psi\pi^+\pi^-\pi^0$ [15], $J/\psi\gamma$ [16] and $\psi'\gamma$ [16], with relative branching ratios

$$\frac{Br(X \to J/\psi\pi^+\pi^-\pi^0)}{Br(X \to J/\psi\pi^+\pi^-)} = 1.0 \pm 0.4 \pm 0.3, \tag{1}$$

$$\frac{Br(X \to J/\psi\gamma)}{Br(X \to J/\psi\pi^+\pi^-)} = 0.33 \pm 0.12, \tag{2}$$

$$\frac{Br(X \to \psi'\gamma)}{Br(X \to J/\psi\pi^+\pi^-)} = 1.1 \pm 0.4. \tag{3}$$

The decay mode $\psi'\gamma$ was further confirmed by the LHCb Collaboration recently [17]. As for the hadronic transition modes, the dipion spectrum in the $J/\Psi\pi^+\pi^-$ is mainly given by ρ^0 resonance whereas the tripion spectrum in $J/\Psi\pi^+\pi^-\pi^0$ comes mainly from the ω meson. The ratio in Eq. (1) shows that these two processes are of the same

* mengce75@pku.edu.cn

† juanj.sanz@uam.es

‡ shimeng1031@pku.edu.cn

§ d.yao@fz-juelich.de

¶ zhenghq@pku.edu.cn

order. One should note that the threshold of $J/\psi\omega$ is about 8 MeV higher than $m_{X(3872)}$, and the width of ω is only about 8 MeV [18]. Thus, the isospin symmetry breaking is not as serious as that shown in Eq. (1) since the phase space of $J/\psi\omega$ decay mode is extremely suppressed compared with that of $J/\psi\rho^0$. Moreover, since the mass of $X(3872)$ is very close to the threshold of $D^0\bar{D}^{*0}$ but not to that of D^+D^{*-}, the rescattering effects through the $D^{(*)}\bar{D}^{(*)}$ loops can generate large isospin symmetry breaking at the amplitude level, and the number in Eq. (1) can be roughly accounted for even if the original decay particle has isospin $I = 0$ [19].

On the theory side, the nature of the $X(3872)$ is still a controversial issue, where different approaches have not reached yet a full agreement. The analysis of Ref. [20–23] favors a $D^0\bar{D}^{*0}/\bar{D}^0D^{*0}$ bound state, as the $X(3872)$ mass is very close to the $D^0\bar{D}^{*0}$ threshold. Other works describe the $X(3872)$ as a $D^0\bar{D}^{*0}/\bar{D}^0D^{*0}$ virtual state [24], a tetraquark [25] or a hybrid state [26]. On the other hand, it has also been considered as a mixture of a charmonium $\chi'_{c1} = \chi_{c1}(2P)$ with a $D^0\bar{D}^{*0}/\bar{D}^0D^{*0}$ component [27, 28]. The mixing can be induced by the coupled-channel effects, and the S-wave $\chi'_{c1} - D\bar{D}^*/\bar{D}D^*$ coupling can also explain the closeness of $m_{X(3872)}$ to the threshold of $D^0\bar{D}^{*0}$ naturally [29, 30]. Furthermore, the existence of the substantial χ'_{c1} component in the $X(3872)$ state is supported by the analyses of the lager production rates of $X(3872)$ both in B decays [27, 31] and at hadron colliders [32].

In Ref. [33], it is proposed to use the pole counting rule [34] to study the nature of X(3872). A couple channel Breit–Wigner propagator is used to describe X(3872) and it is found that two nearby poles are needed in order to describe data. Based on this it is argued that the X(3872) is mainly of $\bar{c}c$ nature heavily renormalized by $\bar{D}D^*$ loop. However, Ref. [33] did not consider the impact effect of the bubble chain generated by $\bar{D}D^*$ loops, which may generate a molecular type pole. Hence it might have been argued that the conclusion made in Ref. [33] was not general. The purpose of this paper is to extend the analysis of Ref. [33] by further including the effect of a contact $\bar{D}D^*$. As we will see later, the major conclusions obtained in Ref. [33] remain unchanged.

In this paper, we only focus on $D^0\bar{D}^{*0}$ and $J/\Psi\pi^+\pi^-$ final states. An effective lagrangian is constructed to calculate the $X(3872)$ decay into $D^0\bar{D}^{*0}$ and $J/\Psi\pi^+\pi^-$. Three different scenarios are taken into consideration to fit experimental data: a single elementary particle $X(3872)$ propagating in the s–channel; only $D\bar{D}^*$ bubble chains with contact $\bar{D}D^*$ rescattering; and the mixed situation, i.e., an elementary $X(3872)$ particle combined with the effect of bubble chain. In Sec. II, the effective lagrangian is introduced and the $B^+ \to K^+D^0\bar{D}^{*0}$ and $B^+ \to K^+J/\Psi\pi^+\pi^-$ amplitudes are calculated. In Sec. III, the numerical fits are performed and the resonance poles are analyzed. A brief summary is provided in Sec. IV. Minor technical details, such as the suppression of the longitudinal component of the amplitude with respect to the transverse one near threshold, are relegated to the appendixes.

II. THEORETICAL ANALYSIS

A.   The Effective Lagrangian

The $X(3872)$ has been identified as a s–wave resonance in the $D^0\bar{D}^{*0}$ and $\bar{D}^0D^{*0}$ final states with isospin $I = 0$, and the similar situation for the p-wave $D\bar{D}$ final states near the $\psi(3770)$ was studied in [35, 36] Likewise, as discussed in the introduction, we will assume $X(3872)$ to be an axial-vector resonance, with $J^{PC} = 1^{++}$. To simplify the notations, from now on the channels $D^0\bar{D}^{*0}/\bar{D}^0D^{*0}$ are labeled just as $D^0\bar{D}^{*0}$, and the channels D^+D^{*-}/D^-D^{*+} are labeled as D^+D^{*-} (unless specifically stated otherwise). Likewise, when the two channels $D^0\bar{D}^{*0}/\bar{D}^0D^{*0}$ and D^+D^{*-}/D^-D^{*+} appear together, they are labeled as $D\bar{D}^*$ in what follows.

In this section we construct the effective lagrangian of the interactions between X(3872) and other particles. The lagrangian of $D\bar{D}^*$ interactions has been constructed by [37–39]. However, operators such as BKX, $BKD\bar{D}^*$, are not considered previously and only constant form factors were used in these previous calculation missing information from B decay vertex.

We will consider a model written in a relativistic form but intended for the description of $D\bar{D}^*$ and $J/\psi\pi^+\pi^-$ invariant energies close to the $D^0\bar{D}^{*0}$ production threshold. We begin by constructing operators in our lagrangian with the lowest number of derivatives and fulfilling invariance under C, P and isospin symmetry. Hence, the interaction between the $X(3872)$ and the $D\bar{D}^*$ pair will occur through the combination of isospin, C and P,

$$X \quad \sim \quad \frac{1}{\sqrt{2}}\left(\bar{D}D^* - \bar{D}^*D\right), \tag{4}$$

where the minus sign stems from the positive $X(3872)$ C–parity and the usual assignment for $D \sim i\bar{q}\gamma_5 c$ and $D^{*\mu} \sim \bar{q}\gamma^\mu c$, with $CD^jC^{-1} = D^{j\,\dagger}$ and $CD_\mu^{j*}C^{-1} = -D_\mu^{j*\,\dagger}$, where j indicates the type of D or D^* meson (e.g. $D^j = D^0, D^+$,etc) [40]. The $SU(2)$ vectors D and D^* gather the isospin doublets [41], $D = \left(\begin{smallmatrix} -D^+ \\ D^0 \end{smallmatrix}\right)$, $D^* = \left(\begin{smallmatrix} -D^{*+} \\ D^{*0} \end{smallmatrix}\right)$, with the transposed conjugates $\bar{D} = (-D^- \quad \bar{D}^0)$, $\bar{D}^* = (-D^{*-} \quad \bar{D}^{*0})$. Hence, following the previous symmetry

prescriptions we consider the isospin, C and P invariant effective lagrangian given by the operators,

$$
\begin{aligned}
\mathcal{L}_{D\bar{D}^*} &= \lambda_1(\bar{D}^{*\mu}D\bar{D}^{*\mu}D + \bar{D}D^{*\mu}\bar{D}D^{*\mu}) + \lambda_2(\bar{D}^{*\mu}D\bar{D}D^{*\mu}), \\
\mathcal{L}_{XD\bar{D}^*} &= g_1 X^\mu(\bar{D}D^*_\mu - \bar{D}^*_\mu D), \\
\mathcal{L}_{BXK} &= ig_2 X^\mu(\overline{B}\partial_\mu K + \text{h.c.}), \\
\mathcal{L}_{BKD\bar{D}^*} &= ig_3(\bar{D}D^*_\mu - \bar{D}^*_\mu D)(\overline{B}\partial^\mu K + \text{h.c.}),
\end{aligned}
\tag{5}
$$

with the isospin doublets $B = \begin{pmatrix} B^+ \\ B^0 \end{pmatrix}$ and $K = \begin{pmatrix} K^+ \\ K^0 \end{pmatrix}$. In the present model they are combined in such a way that the charge of the outgoing kaon always coincides with the charge of the incoming B-meson, as we are interested in processes where the remaining decay product state is neutral and isoscalar (the quantum numbers of the $X(3872)$). In addition to Eq. (5), for the decay into $B^+ \to K^+ J/\psi\rho\,(\omega)$ we have the following operators,

$$
\begin{aligned}
\mathcal{L}_{X\Psi V} &= ig_4 X^\mu \Psi^\nu \partial^\alpha V^\beta \epsilon_{\mu\nu\alpha\beta}, \\
\mathcal{L}_{\Psi V D\bar{D}^*} &= ig_5(\bar{D}D^{*\mu} - \bar{D}^{*\mu}D)\Psi^\nu \partial^\alpha V^\beta \epsilon_{\mu\nu\alpha\beta},
\end{aligned}
\tag{6}
$$

with V denoting $\rho(770)$ or $\omega(782)$. In principle, one may also have a direct $\bar{B}K\Psi V$ decay through the corresponding operator. However, since we are interested in the $X(3872)$–resonant structure, we will not discuss this term in the lagrangian since it only contributes to the background term. The couplings have dimensions $[g_1] = E^1$ and $[g_3] = [g_5] = E^{-1}$ while the other coupling constants are dimensionless.

The general structure of $\mathcal{L}_{D\bar{D}^*}$ contains two coupling constants λ_1 and λ_2, being consistent with heavy quark symmetry [37]. They provide the contact $D\bar{D}^*$ rescattering. Operators with higher derivatives are regarded as corrections in this model and will be neglected. It is convenient to expand the operator $\mathcal{L}_{XD\bar{D}^*}$ together with the Lagrangian $\mathcal{L}_{D\bar{D}^*}$ in the explicit form

$$
T_{D\bar{D}^*} = \begin{pmatrix}
T_{D^{*-}D^+D^{*-}D^+} & T_{D^{*-}D^+D^{*+}D^-} & T_{D^{*-}D^+\bar{D}^{*0}D^0} & T_{D^{*-}D^+D^{*0}\bar{D}^0} \\
T_{D^{*+}D^-D^{*-}D^+} & T_{D^{*+}D^-D^{*+}D^-} & T_{D^{*+}D^-+\bar{D}^{*0}D^0} & T_{D^{*+}D^-D^{*0}\bar{D}^0} \\
T_{\bar{D}^{*0}D^0D^{*-}D^+} & T_{\bar{D}^{*0}D^0D^{*+}D^-} & T_{\bar{D}^{*0}D^0\bar{D}^{*0}D^0} & T_{\bar{D}^{*0}D^0D^{*0}\bar{D}^0} \\
T_{D^{*0}\bar{D}^0D^{*-}D^+} & T_{D^{*0}\bar{D}^0D^{*+}D^-} & T_{D^{*0}\bar{D}^0\bar{D}^{*0}D^0} & T_{D^{*0}\bar{D}^0D^{*0}\bar{D}^0}
\end{pmatrix} = \begin{pmatrix}
2\lambda_1 & \lambda_2 & 2\lambda_1 & \lambda_2 \\
\lambda_2 & 2\lambda_1 & \lambda_2 & 2\lambda_1 \\
2\lambda_1 & \lambda_2 & 2\lambda_1 & \lambda_2 \\
\lambda_2 & 2\lambda_1 & \lambda_2 & 2\lambda_1
\end{pmatrix},
$$

$$
\vec{\mathcal{F}}_{X^\mu \to D\bar{D}^*} = \begin{pmatrix}
\mathcal{F}_{X^\mu \to D^{*-}D^+} \\
\mathcal{F}_{X^\mu \to D^{*+}D^-} \\
\mathcal{F}_{X^\mu \to \bar{D}^{*0}D^0} \\
\mathcal{F}_{X^\mu \to D^{*0}\bar{D}^0}
\end{pmatrix} = g_1\,\vec{u}_X, \qquad \text{with } \vec{u}_X = \begin{pmatrix} 1 \\ -1 \\ 1 \\ -1 \end{pmatrix}.
\tag{7}
$$

However, in order to match the $D^0\bar{D}^{*0}/\bar{D}^0 D^{*0}$ non-relativistic effective field theory near threshold (the minimal charm meson model) [38], one needs $\lambda_2 = -2\lambda_1$. Hence, under this condition the $T_{D\bar{D}^*}$ gets the simplified form:

$$
T_{D\bar{D}^*} = \lambda_2\,\vec{u}_X\,\vec{u}_X^T.
\tag{8}
$$

Notice that this contact scattering matrix $T_{D\bar{D}^*}$ projects into the flavor structure of the $X \to D\bar{D}^*$ transition. Hence, it accounts only for the $D\bar{D}^*$ local rescattering with the quantum number of the $X(3872)$. From now on, we will use $\lambda_2 = -2\lambda_1$ all along the article.

B. Amplitude of $B^+ \to K^+ D^0 \bar{D}^{*0}$

Based on the lagrangian in Eqs. (5) and (6), we extract the decay amplitude $B^+ \to K^+ D^0 \bar{D}^{*0}$. Fig. 1 shows the interaction vertices and Fig. 2 describes Feynmann diagrams for $B^+ \to D^0\bar{D}^{*0}K^+$ and $B^+ \to J/\Psi\pi^+\pi^- K^+$. In the first line of the Fig. 2, one can observe the $D\bar{D}^*$ final state interaction coming in part from a bubble chain of local scatterings through the λ_2 operator. In general, every rescattering is produced by two kinds of interactions: contact interaction and $X(3872)$ exchanges in the s–channel. The rescattering effective vertex denoted as (3) in Fig. 1 is given by

$$
iA_{D\bar{D}^*}^{\mu\nu} = ig^{\mu\nu}T_{D\bar{D}^*} + i(g_1)^2 D(p^2)^{\mu\nu}(\vec{u}_X\vec{u}_X^T) = \left[i\lambda_2 g^{\mu\nu} + \frac{ig_1^2(g^{\mu\nu} - \frac{p^\mu p^\nu}{M_X^2})}{p^2 - M_X^2} \right](\vec{u}_X\vec{u}_X^T),
\tag{9}
$$

where $p = p_D + p_{\bar{D}^*}$ is the momentum of the $D\bar{D}^*$ system, and M_X the $X(3872)$ mass, λ_2 provides the local scattering of the $D\bar{D}^*$ meson pairs and $(\vec{u}_X\vec{u}_X^T)$ provides the precise structure for the various flavor scatterings. For a massive particle, like the X(3872), the Proca propagator has two components,

$$
D(p^2)^{\mu\nu} = \frac{-i(g^{\mu\nu} - \frac{p^\mu p^\nu}{M_X^2})}{p^2 - M_X^2} = \frac{-iP_T^{\mu\nu}(p)}{p^2 - M_X^2} + \frac{iP_L^{\mu\nu}(p)}{M_X^2},
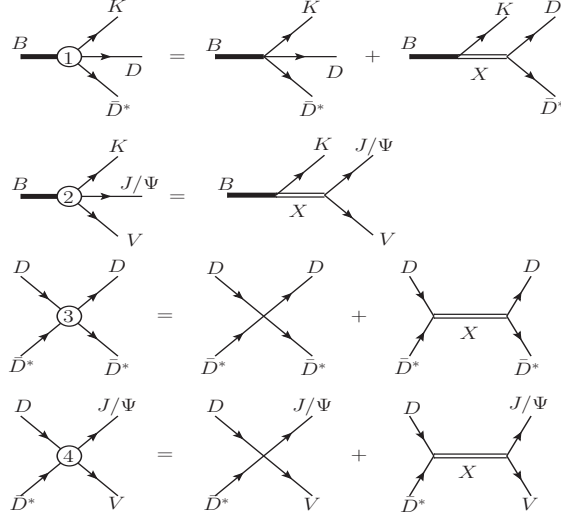\tag{10}
$$

FIG. 1: Interaction vertices. The blob (1) depends on the couplings $g_1 \cdot g_2$ and g_3, the blob (2) depends on $g_2 \cdot g_4$, the blob (3) depends on λ_2 and g_1^2, and the blob (4) depends on g_5 and $g_1 \cdot g_4$.
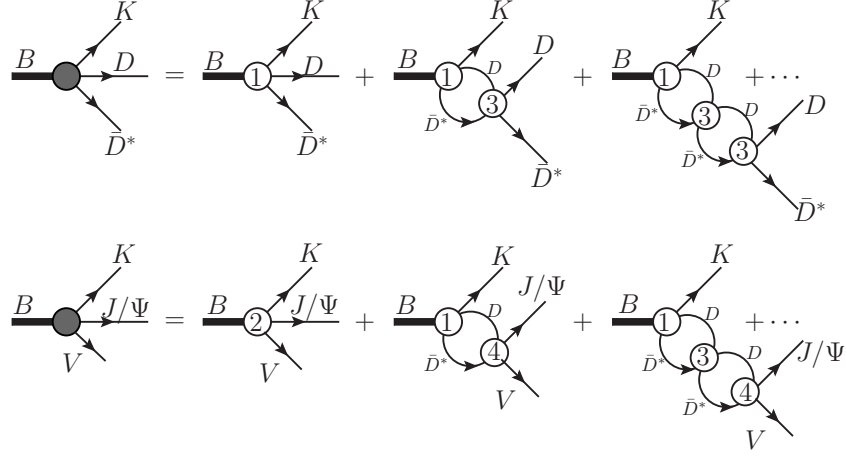

FIG. 2: Decay diagrams.

with $P_{T\mu\nu} = g_{\mu\nu} - \frac{p_\mu p_\nu}{p^2}$ and $P_{L\mu\nu} = \frac{p_\mu p_\nu}{p^2}$ the transverse and longitudinal projection operators, respectively. The longitudinal part happens to be suppressed in the $D\bar{D}^*$ decay by an extra factor $|\vec{p}_{D^*}|$ near the $D\bar{D}^*$ threshold and will produce a much smaller impact. Thus, no pole will be generated in the longitudinal channel in the neighbourhood of the $D\bar{D}^*$ threshold. Detailed discussion on this point can be found in Appendix A. The effective vertices in the blobs (1) and (4) in Fig. 1 also have contact interaction and $X(3872)$ exchanges. However, in the effective vertex (2) only $X(3872)$ exchanges have been taken into account in our model. Possible contact interactions will be treated as background to the spectrum in our later phenomenological analysis.

After taking into account the $D\bar{D}^*$ rescattering effect, the $B^+ \to D^0 \bar{D}^{*0} K^+$ decay amplitude can be separated into transverse and longitudinal components,

$$\mathcal{M}_{D^0\bar{D}^{*0}} = -\frac{(g_3 + \frac{g_1 g_2}{s-M_X^2})p_K^\mu \epsilon_{\bar{D}^*}^\nu}{1 - (i\lambda_2 + i\frac{g_1^2}{s-M_X^2})\hat{\Pi}_T(s)}P_{T\mu\nu}(p) + \frac{(g_3 + \frac{g_1 g_2}{M_X^2})p_K^\mu \epsilon_{\bar{D}^*}^\nu}{1 - (i\lambda_2 + i\frac{g_1^2}{M_X^2})\hat{\Pi}_L(s)}P_{L\mu\nu}(p), \tag{11}$$

where M_X, p_K and $\epsilon_{\bar{D}^{*0}}$ are the mass of X(3872), the momentum of K meson and the $\bar{D}^{*0}$ polarization, respectively, and $s = p^2$. The total one-loop contributions are given by $\hat{\Pi}_T = 2(\hat{\Pi}_{T_{D^0\bar{D}^{*0}}} + \hat{\Pi}_{T_{D^+D^{*-}}})$ and $\hat{\Pi}_L = 2(\hat{\Pi}_{L_{D^0\bar{D}^{*0}}} + \hat{\Pi}_{L_{D^+D^{*-}}})$. The factor 2 results from the identity between the $D\bar{D}^*$ and $\bar{D}D^*$ contributions. For instance, the $D^0\bar{D}^{*0}$

one loop integral is given by

$$\int \frac{d^D k}{(2\pi)^D} \frac{g_{\mu\nu} - \frac{k_\mu k_\nu}{m_{D^{*0}}^2}}{(k^2 - m_{D^{*0}}^2)((p-k)^2 - m_{D^0}^2)} = P_{T\mu\nu}(p)\Pi_{T_{D^0\bar{D}^{*0}}}(s) + P_{L\mu\nu}(p)\Pi_{L_{D^0\bar{D}^{*0}}}(s).$$

(12)

The contributions $\Pi_{T_{D^+D^{*-}}}(s)$ and $\Pi_{L_{D^+D^{*-}}}(s)$ have similar structure but with charged $D\bar{D}^*$ masses instead of neutral, having thus a different production threshold $\sqrt{s} = 3879.4$ MeV. The $D^0\bar{D}^{*0}$ threshold is placed at $\sqrt{s} = 3871.3$ MeV, 8 MeV below the charged one. The expressions of $\hat{\Pi}_{T_{D^0\bar{D}^{*0}}}(s)$ and $\hat{\Pi}_{L_{D^0\bar{D}^{*0}}}(s)$ are given in Appendix B. Therein, $\hat{\Pi}_{T_{D^0\bar{D}^{*0}}}(s)$ and $\hat{\Pi}_{L_{D^0\bar{D}^{*0}}}(s)$ are proven to be, respectively, proportional to $-\frac{1}{16\pi}\rho(s)$ and $\frac{1}{16\pi}\rho^3(s)$ near the $D^0\bar{D}^{*0}$ threshold, with $\rho(s) = \frac{2|\vec{p}_D|}{\sqrt{s}} = \frac{\sqrt{(s-(m_{D^0}+m_{D^{*0}})^2)(s-(m_{D^0}-m_{D^{*0}})^2)}}{s}$, being $\vec{p}_D$ here the D three-momentum in the $D\bar{D}^*$ center-of-mass rest frame.

There are also other decay channels with much lighter production thresholds, such as $J/\Psi\gamma$, etc, which affect the $X(3872)$ propagator. Since all such channel thresholds are far away from the $D^0\bar{D}^{*0}$ one and the energy region under study is a narrow range around the latter, the contributions to the $X(3872)$ self energies from these channels can be fairly approximated as a constant. In order to account for these absorptive contributions, in the transverse part of the amplitude in Eq. (11) we make the replacement

$$s - M_X^2 \Rightarrow s - M_X^2 + i M_X (\Gamma_{J/\Psi\pi\pi}(s) + \Gamma_{J/\Psi\pi\pi\pi}(s) + \Gamma_0),$$

(13)

where the effective parameters M_X and Γ_0 will be determined by our fits to experimental data, and $\Gamma_{J/\Psi\pi\pi}(s)$ and $\Gamma_{J/\Psi\pi\pi\pi}(s)$ are the partial widths of the X(3872) from $J/\Psi\rho$ and $J/\Psi\omega$ contribution. We denote the $XJ/\Psi\omega$ coupling as g_4' to distinguish it from the $XJ/\Psi\rho$ coupling, denoted as g_4. The widths $\Gamma_{J/\Psi\pi\pi}(s)$ and $\Gamma_{J/\Psi\pi\pi\pi}(s)$ are

$$\Gamma_{J/\Psi\pi\pi}(s) = g_4^2 \int_{2m_\pi}^{\sqrt{s}-m_{J/\Psi}} \frac{dm}{2\pi} \frac{k(m)(\frac{s\cdot k(m)^2}{m_{J/\Psi}^2} + 2m_{J/\Psi}^2 + 2s - 6\sqrt{s}k(m) + k(m)^2)\Gamma_\rho}{4\pi s((m-m_\rho)^2 + \Gamma_\rho^2/4)},$$

(14)

$$\Gamma_{J/\Psi\pi\pi\pi}(s) = g_4'^2 \int_{3m_\pi}^{\sqrt{s}-m_{J/\Psi}} \frac{dm}{2\pi} \frac{k(m)(\frac{s\cdot k(m)^2}{m_{J/\Psi}^2} + 2m_{J/\Psi}^2 + 2s - 6\sqrt{s}k(m) + k(m)^2)\Gamma_\omega}{4\pi s((m-m_\omega)^2 + \Gamma_\omega^2/4)},$$

(15)

where $k(m) = \sqrt{\frac{(s-(m+m_{J/\Psi})^2)(s-(m-m_{J/\Psi})^2)}{4s}}$, $m_{J/\Psi}$, m_ρ, m_ω and Γ_ρ, Γ_ω are the mass of J/Ψ, ρ, ω and the width of ρ, ω respectively.

The $D^0\bar{D}^{*0}$ invariant mass spectrum is provided by

$$\frac{dN}{dm_{D^0\bar{D}^{*0}}} = N_1 \frac{d\Gamma}{dm_{D^0D^{*0}}} = N_1 \frac{2m_{D^0\bar{D}^{*0}}}{(2\pi)^3 32 M_B^3} \int (|\mathcal{M}_{D^0\bar{D}^{*0}}|^2)dm_{DK}^2 + c_1\rho_3(s),$$

(16)

where m_{DK} is the invariant mass of the DK^+ system; N_1 is a normalization factor; c_1 is a constant, which multiplies the phase space ($\rho_3(s) = |\vec{p}_k||\vec{p}_{DD^*}|$) and models the background contribution.

C. $B^+ \to K^+ J/\Psi\pi^+\pi^-$ amplitude

In the $J/\Psi\pi^+\pi^-K^+$ situation, we assume that the B^+ meson firstly decays into $K^+ J/\Psi V$, and then V decays into $\pi^+\pi^-$. The vertices are presented in Fig.1. As explained before, no $BKJ/\Psi V$ contact interaction is considered in the present study. It is assumed to be part of the constant background term below.

In the second line of Fig. 2 we show only the $D\bar{D}^*$ final state interaction. As the energy range under study is very close to the $D\bar{D}^*$ threshold, the $D\bar{D}^*$ rescattering dependence on the energy and other channels are accounted through the constant width Γ_0 introduced in the above section in Eq. (13) together with the $\Gamma_{J/\Psi\pi\pi}$ and $\Gamma_{J/\Psi\pi\pi\pi}$ contributions therein.

The $B^+ \to J/\Psi V K^+$ amplitude is now given by the much involved expression as the following:

$$\mathcal{M}_{J/\Psi V} =$$
$$\frac{p_K^\mu \epsilon_\Psi^\nu p_V^\alpha \epsilon_V^\beta \epsilon_{\rho\nu\alpha\beta}(g_2 g_4(1 - i\lambda_2\hat{\Pi}_T) + ig_1 g_2 g_5\hat{\Pi}_T + ig_3 g_5(s - M_X^2)\hat{\Pi}_T + ig_1 g_3 g_4\hat{\Pi}_T)}{(s - M_X^2)(1 - i\lambda_2\hat{\Pi}_T) - ig_1^2\hat{\Pi}_T} P_{T\mu}^\rho(p)$$

$$+ i\, g_3 p_K^\mu \hat{\Pi}_L \epsilon_\Psi^\nu p_V^\alpha \epsilon_V^\beta \epsilon_{\rho\nu\alpha\beta} \frac{ig_5 - \frac{ig_1 g_4}{M_X^2}}{1 - (i\lambda_2 - \frac{ig_1^2}{M_X^2})\hat{\Pi}_L} P_{L\mu}^\rho(p) - \frac{ig_2 p_K^\mu(g_4 + \frac{ig_1 g_5\hat{\Pi}_L}{1 - i\lambda_2\hat{\Pi}_L})\epsilon_\Psi^\nu p_V^\alpha \epsilon_V^\beta \epsilon_{\rho\nu\alpha\beta}}{M_X^2 + \frac{ig_1^2\hat{\Pi}_L}{1 - i\lambda_2\hat{\Pi}_L}} P_{L\mu}^\rho(p),$$

(17)

where p_V and ϵ_V are the momentum and the polarization of V meson, and ϵ_Ψ is the polarization of J/Ψ. The other symbols are the same as in Eq. (11), and the $s - M_X^2$ also needs to be replaced by $s - M_X^2 + iM_X(\Gamma_{J/\Psi\pi\pi}(s) + \Gamma_{J/\Psi\pi\pi\pi}(s) + \Gamma_0)$ as before.

An adequate determination of the decay into $J/\Psi\pi^+\pi^-$ amplitude can be extracted from the $B^+ \to J/\Psi V K^+$ amplitude by inserting the propagator of the V particle, the $\rho(770)$, as discussed in previous sections. The $J/\Psi\pi^+\pi^-$ is studied for the $B^+ \to J/\Psi\pi^+\pi^- K^+$ decay. Considering the cascade decay $B^+ \to K^+ J/\Psi V \to K^+ J/\Psi\pi\pi$, the spectrum is given by [18]

$$
\begin{aligned}
\frac{dN}{dm_{J/\Psi\pi\pi}} &= N_2 \int_{2m_\pi}^{m_{J/\Psi V} - m_{J/\Psi}} \frac{d\Gamma}{dm_{J/\Psi V}} \frac{k(m_{\pi\pi})\,\Gamma_V}{(m_{\pi\pi} - m_V)^2 + \Gamma_V^2/4} dm_{\pi\pi} \;+\; c_2 \\
&= N_2 \int\int \frac{2m_{J/\Psi V}}{(2\pi)^3 32 M_B^3} |\mathcal{M}_{J/\Psi V}|^2 dm_{J/\Psi K}^2 \frac{k(m_{\pi\pi})\Gamma_V}{(m_{\pi\pi} - m_V)^2 + \Gamma_V^2/4} dm_{\pi\pi} \;+\; c_2,
\end{aligned}
\tag{18}
$$

where N_2 is the normalization constant, c_2 parametrizes the background, $m_{\pi\pi}$ is the $\pi^+\pi^-$ invariant mass and $k(m_{\pi\pi})$ is the pion three-momentum in the $\pi^+\pi^-$ rest-frame. The constants m_V and Γ_V are the mass and width of the vector meson, respectively.

III. NUMERICAL RESULTS AND POLE ANALYSIS

A. Fits to the amplitudes

In above sections we have calculated the $B^+ \to D^0\bar{D}^{*0}K^+$ and $B^+ \to J/\Psi\pi^+\pi^-$ invariant mass spectra, taking into account both the Breit–Wigner particle propagation (elementary X(3872)) and the $D\bar{D}^*$ bubble chain mechanisms. In this section we will carefully study the interference and competition between the two mechanisms through a numerical fit to data. We anticipate here the χ^2 prefers the elementary scenario than the molecular one, though the mixed situation (i.e., with both mechanisms involved) may not be excluded.

We perform the following three fits:

- Case I: We assume that $D\bar{D}^*$ loops only renormalized the X(3872) self-energy through $XD\bar{D}^*$ vertex with coupling constant g_1. There is no $D\bar{D}^*$ contact interaction and $\lambda_2 = 0$ in Eqs. (11) and (17). This situation implies that there is a pre-existent elementary X(3872), which is not a molecular bound state generated by $D\bar{D}^*$ intermediate state.

- Case II: Among the interactions in Fig. 1 only the direct $D\bar{D}^*$ local interaction is taken into account and intermediate $X(3872)$ exchanges are discarded. That means setting g_1, g_2, $g_4 = 0$ in amplitudes (11) and (17), and corresponds to the situation where the $D\bar{D}^*$ bubble loop chains are responsible for the experimentally observed peak, i.e., since line-shape and pole are both related but what generates both is the bubble chain.

In such a situation, the structure of amplitudes takes then the form

$$
\frac{f_T}{\lambda_2^{-1} - i\hat{\Pi}_T} \;+\; \frac{f_L}{\lambda_2^{-1} - i\hat{\Pi}_L},
\tag{19}
$$

where f_T and f_L denote the corresponding numerators in the amplitudes. When there is the X propagation (Case I), the contributions from other channels, such as $J/\Psi\gamma$, are taken into account through the constant width Γ_0 in the X propagator. In the present situation (Case II) there is no intermediate $X(3872)$ elementary particle, the contributions from other channels are taken into consideration by shifting the coupling constant λ_2 to λ_{eff}:

$$
\frac{1}{\lambda_{eff}} = \frac{1}{\lambda_2} + ic_0,
\tag{20}
$$

where c_0 is a real constant which accounts for lower thresholds contributions. The role of ic_0 is to shift the pole from real axis to the complex plane (i.e., contributes a small width to the bound state). Now the amplitude takes the form:

$$
\frac{f_T}{\lambda_2^{-1} - i\hat{\Pi}_T} \;+\; \frac{f_L}{\lambda_2^{-1} - i\hat{\Pi}_L}, \to \frac{f_T}{\lambda_2^{-1} + ic_0 - i\hat{\Pi}_T} + \frac{f_L}{\lambda_2^{-1} + ic_0 - i\hat{\Pi}_L}.
\tag{21}
$$

As $\hat{\Pi}_T \propto -\rho(s)$ near the $D\bar{D}^*$ threshold, the pole in the transverse component is determined by the sign of λ_2, which will be discussed in the next subsection.

- Case III: We also tried to incorporate both fit I and fit II features by switching on all the interactions in Figs. 1 and 2, allowing both direct contact interactions and $X(3872)$ intermediate state exchanges in the s–channel. However, as we will see later, this does not improve the total χ^2 with respect to Case I.

In next subsection we will try to examine which of the above scenario is favored by experimental data.

B. Data fitting

Using Eqs. (16) and (18), we proceed now to fit two sets of $D^0 \bar{D}^{*0}$ data and two of $J/\Psi \pi^+ \pi^-$ data. The two sets of $D^0 \bar{D}^{*0}$ data are: $B^+ \to X K^+ \to D^0 \bar{D}^{*0} K^+$ from BELLE [14] and the $B^+ \to X K^+ \to D^0 \bar{D}^{*0} K^+$ from BABAR [13]. The D^{*0} and $\bar{D}^{*0}$ are reconstructed from $D^0 \pi^0, D^0 \gamma$ and $\bar{D}^0 \pi^0, \bar{D}^0 \gamma$, respectively. We perform our fits from the $D^0 \bar{D}^{*0}$ threshold up to $\sqrt{s} = 3893.8$ MeV for BELLE and $\sqrt{s} = 3895$ MeV for BABAR. There are also two $J/\Psi \pi^+ \pi^-$ data samples (BELLE [12] and BABAR [11]). We fit from $\sqrt{s} = 3843.4$ MeV up to 3892.4 MeV for BELLE [12] and from $\sqrt{s} = 3847.2$ MeV up to 3897.6 MeV for BABAR [11].

As explained in the previous subsection, we consider three fit cases: Pure elementary particle (Fit I), where we set $\lambda_2 = 0$ (and of course $c_0 = 0$); Pure molecule picture (Fit II), where g_1, g_2 and g_4 are set to zero; and a mixing of the elementary particle and molecule state (Fit III), where we have all the parameters except c_0 in Table I, with λ_2 real. Unfortunately, the Fit III was found to be unstable: Since too many parameters are involved, no convergent solution is found with positive error matrix. The total χ^2 is not meaningfully improved in comparison to Fit I. Hence we will focus mainly on the first two fits and relegate the discussion in the following.

The most important parameters for the X(3872) pole position are the two coupling constants λ_2, g_1 and M_X. The fitting results are presented in Table I. The N_{1i}(i=1,2,3) and N_{2i}(i=1,2) are normalization constants for the $D^0 \bar{D}^{*0}$ and $J/\Psi \pi^+ \pi^-$ processes, and the c_{1i}(i=1,2,3) and c_{2j} $(j = 1, 2)$ parameterize the background contributions for the $B^+ \to K^+ D^0 \bar{D}^{*0}$ and $B^+ \to K^+ J/\Psi \pi^+ \pi^-$ data, respectively. Since each spectrum has a different normalization constant N_{ij}, in general it is not really possible to determine the N_{ij} and the couplings g_2, g_3 and g_5, independently.
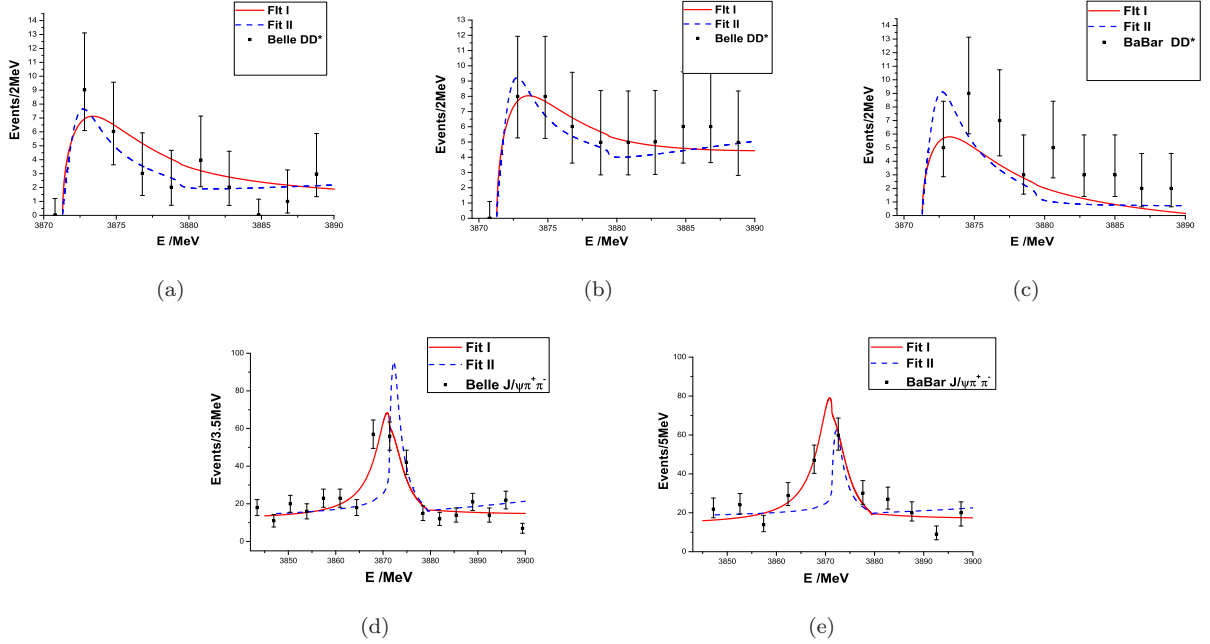

(a) (b) (c)

(d) (e)

FIG. 3: (a), (b), $D^0 \bar{D}^{*0}$ invariant mass spectrum for BELLE data. The $\bar{D}^*$ are reconstructed from $\bar{D}^0 \gamma$ and $\bar{D}^0 \pi^0$, respectively in (a) and (b). (c), $D^0 \bar{D}^{*0}$ invariant mass spectrum for BABAR data. (d), (e), $J/\Psi \pi^+ \pi^-$ invariant mass spectrum for BELLE and BABAR data, respectively. Here $E = \sqrt{s}$.

In Table I, the $N_{ij} g_3^2$ are obviously larger in Fit II than in Fit I. This is due to the contributions proportional g_1 and g_2 in Fit I, which are absent in Fit II and have to be compensated by large values of $N_{1j} g_3^2$ and $N_{2j} g_3^2 g_5^2$.

The fits of the theoretical expressions (16) and (18) to data are shown in Fig. 3. Fit I has a much smaller χ^2 per degree of freedom (d.o.f.) than that of Fit II. This indicates that the model with bubble chains with contact $D\bar{D}^*$

	Fit I	Fit II
	$\chi^2/dof = 47.1/(60-17)$	$\chi^2/dof = 83.3/(60-12)$
λ_2	–	552.7 ± 1.1
c_0	–	$(1.70\pm 0.01)\times 10^{-4}$
g_1 (MeV)	1977 ± 908	–
g_2/g_3 (MeV)	196 ± 52	–
g_4	0.27 ± 0.08	–
g_4'	0.44 ± 0.11	–
g_5 (MeV^{-1})	0.016 ± 0.014	1.0 (fixed)
M_X(MeV)	3870.3 ± 0.5	–
Γ_0(MeV)	4.3 ± 1.5	–
$N_{11}\cdot g_3^2(10^{-3}\mathrm{MeV}^{-3})$	9.2 ± 5.0	159 ± 55
$N_{12}\cdot g_3^2(10^{-3}\mathrm{MeV}^{-3})$	8.1 ± 4.0	181 ± 53
$N_{13}\cdot g_3^2(10^{-3}\mathrm{MeV}^{-3})$	9.1 ± 4.7	143 ± 48
$N_{21}\cdot g_3^2\ (10^{-5}\mathrm{MeV}^{-4})$	4.7 ± 1.3	63 ± 35
$N_{22}\cdot g_3^2\ (10^{-5}\mathrm{MeV}^{-4})$	3.9 ± 117	116 ± 33
$c_{11}\times 10^5$	3.4 ± 1.7	3.6 ± 1.4
$c_{12}\times 10^5$	1.9 ± 1.0	0.4 ± 0.2
$c_{13}\times 10^5$	1.6 ± 1.2	1.1 ± 1.0
c_{21}	15.5 ± 2.1	15.1 ± 2.0
c_{22}	13.1 ± 1.5	12.6 ± 1.4

TABLE I: Fit parameters for the two different scenarios. In Fit II the entry $N_{2j}g_3^2$ corresponds to $N_{2j}g_3^2g_5^2$. The fits only depend on $N_{ij}g_3^2$, g_2/g_3 and g_5 in Fit I, and $N_{ij}g_3^2g_5^2$ for Fit II ($g_2 = 0$ in this Fit). At the practical level, we will fix $g_5 = 1$ in the Fit II and the entry for $N_{2j}g_3^2$ must be understood as the fit value for $N_{2j}g_3^2g_5^2$.

rescattering alone is not favored by experimental data. It is worth mentioning that, compared with Fit I, the χ^2/d.o.f. of Fit III is slightly better, but at present stage we are not able to draw a definitive conclusion from this study.

One can observe an obvious cusp structure at $\sqrt{s} = 3879.4$ MeV in Fig. 3. This is due to the effect of the $D^\pm D^{*\mp}$ threshold in the coupled channel analysis performed in this article, where the interference with the charged channel is taken into account [42].

The energy resolution was also considered in a comparative fit. Nevertheless, the fit results were not sensitive to it. We also investigated the longitudinal component of the amplitudes. We find that the poles in the longitudinal components are spurious and are always found very far away from the energy region under study. Hence the longitudinal part can only be considered as a part of the background contribution.

C. Pole analysis

In the most general case, Fit III, the denominators of the transverse and longitudinal parts can be written as

$$(s - M_X^2 + iM_X(\Gamma_{J\pi\pi}(s) + \Gamma_{J\pi\pi\pi}(s) + \Gamma_0))(1 - i\lambda_2\hat{\Pi}_T(s)) - ig_1^2\hat{\Pi}_T(s)\,, \qquad (22)$$

$$M_X^2(1 - i\lambda_2\hat{\Pi}_L(s)) - ig_1^2\hat{\Pi}_L(s)\,. \qquad (23)$$

We have the same structure for Fit I, but with λ_2 set to zero. On the other hand, in the Fit II case, the $X(3872)$ particle propagator is absent and we have transverse and longitudinal denominators of the form

$$\lambda_2^{-1} + ic_0 - i\hat{\Pi}_T(s)\,, \qquad (24)$$

$$\lambda_2^{-1} + ic_0 - i\hat{\Pi}_L(s)\,. \qquad (25)$$

Near threshold we have $\hat{\Pi}_T = \frac{1}{16\pi}(-\rho(s) + O(\rho^2(s)))$ and $\hat{\Pi}_L = \frac{1}{16\pi}(\rho^3(s) + O(\rho^4(s)))$ (a proof can be found in App. B). Thus, the transverse and the longitudinal components have different pole locations on the complex energy plane.

	sheet I	sheet II	sheet III	sheet IV
$\rho_{D^0 D^{*0}}(s)$	+	-	-	+
$\rho_{D^+ D^{*-}}(s)$	+	+	-	-

TABLE II: Definition of the four Riemann sheets with the $D^0 \bar{D}^{*0}$ and $D^+ D^{*-}$ channels. The $\rho_{D^0 D^{*0}}(s)$ and $\rho_{D^+ D^{*-}}(s)$ represent the $\rho(s)$ for each channel in $\hat{\Pi}_T$ and $\hat{\Pi}_L$.

Sheet	Fit I	Fit II
I	3871.1-3.3i	–
II	3870.5-3.7i	3871.7-0.9i
III	3869.0-4.0i	–
IV	3869.8-3.5i	–

TABLE III: Transverse pole position of the $X(3872)$ for the two fits. The value of $\sqrt{s_{\text{pole}}} = M_{\text{pole}} - i\Gamma_{\text{pole}}/2$ is given in MeV. No pole is found in the sheets I, III and IV for Fit II. Since there are lower thresholds, such as $J/\Psi\gamma$, the pole on sheet I does not break the causality.

If we focus our attention on just the $D^0 \bar{D}^{*0}$ and $D^+ D^{*-}$ channels, with the threshold at $\sqrt{s} = 3871.3$ MeV and $\sqrt{s} = 3879.4$ MeV, respectively, the complex Riemann surface is divided into four sheets. The $\rho(s)$–sign prescriptions to pass from one Riemann sheet to another are provided in Table II. One should notice that, in addition to the $D^0 \bar{D}^{*0}$ and $D^+ \bar{D}^{*-}$ channels, there are $J/\Psi\pi\pi$, $J/\Psi\pi\pi\pi$ and other channels represented by Γ_0, which have lower thresholds. To simplify the discussion, only the near $X(3872)$ resonance channels $D^0 \bar{D}^{*0}$ and $D^+ \bar{D}^{*-}$ are considered to classify the Riemann sheets. The pole positions of the transverse part are presented in Tables III. Poles from the longitudinal part are far away from the physical region and, hence, are spurious and have noting to do with physics under concern.

In Fit I, four poles are found, with similar widths of approximately 6 MeV, mainly generated from the elementary component of the X(3872). Other channels ($J/\Psi\pi\pi, J/\Psi\gamma$) were also taken into account in Fit I through the $\Gamma_{J/\Psi\pi\pi}$, $\Gamma_{J/\Psi\pi\pi\pi}$ and the parameter Γ_0 in the propagator of the $X(3872)$, respectively. They have much lighter thresholds than the $D^0 \bar{D}^{*0}$ one and vary smoothly in the small energy region under study. A large elementary particle component for the $X(3872)$ is hinted by the poles on the four Riemann sheets that can be found in Table III for Fit I, in agreement to the findings in Ref. [43].

In Fit II, there is only one transverse pole, determined through Eq. (24) and located on the 2nd Riemann sheet, with a width $\Gamma_{\text{pole}} = 1.8$ MeV slightly smaller than those in Fit I.

As discussed above, the transverse part of the loop has the near threshold behaviour $\hat{\Pi}_T \propto -\rho(s)$. Thus, the coupling λ_2 determines the pole position. In the Fit II scenario, we only find a pole in the 2nd Riemann sheet, which means the $X(3872)$ would not be a bound state but a virtual state.

D. Fit III Pole Moving

In the sections above, only Fit I and Fit II were discussed. Instead, Fit III (a combination of Fit I and Fit II) does not give a very different χ^2/d.o.f. comparing with Fit I, which changes from 47.1/43 to 42.4/42. The parameters $g_1 = 2320 \pm 291$MeV, $g_4 = 0.18 \pm 0.09$, $g_4' = 0.32 \pm 0.27$, $M_X = 3874.2 \pm 0.8$MeV and $\Gamma_0 = 1.7 \pm 1.4$MeV in Fit III are also similar to those in Fit I, but with the additional coupling $\lambda_2 = 647.1 \pm 26.0$ in Fit III. However, compare with Fit I, the transverse part of the amplitude has an additional pole on the 1st sheet, which is very close to the real axis. That might provide a different physical picture for the nature of the X(3872) if proven true.

By searching the poles the transverse propagator in Fit III in Eq. (22), we found there is one pole on the first sheet ($\sqrt{s} = 3874.1 - 0.5i$ MeV) very close to the real s–axis. In addition to this pole, there is another pair of poles on the 1st and 2nd sheet at $\sqrt{s} = 3869.5 - 0.1i$ MeV and $3874.3 - 2.6i$ MeV, respectively, which are also closer than those of Fit I. The other two poles on sheet III and IV have similar positions as in Fit I but slightly smaller imaginary parts, which are around 2.0 MeV. Obviously, the presence of poles on the first sheet would lead to important effects which should be analyzed carefully.

Since the additional pole on the first sheet is the main difference between Fit III and Fit I, one straightforwardly may suppose that the additional pole comes from $D\bar{D}^*$ rescattering. To confirm this guess, we vary the coupling constant λ_2 to find out whether the poles are affected by this coupling constant. We define the scale factor x in the
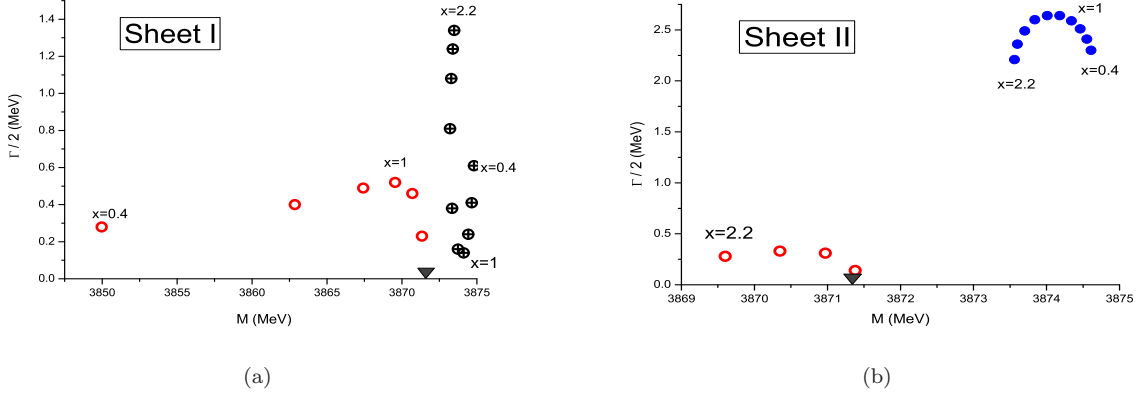
FIG. 4: Pole trajectories for x varied in the range [0.4, 2.2], with $\lambda_2 = 647.1x$. All the other parameters remain fixed at their respective values from Fit III. $x = 1$ corresponds to the λ_2 central value in Fit III.

form $\lambda_2 = 647.1x$ (with $x = 1$ corresponding to the central value in Fit III), which is varied in the range $x \in [0,4, 2.2]$ in steps of 0.2. The trajectories of poles are shown in Fig. 4. It reveals that although the elementary $X(3872)$ plays a main role in the propagator, the contact $D\bar{D}^*$ rescattering becomes important as x increasing. There is a 1st sheet pole from far below the $D^0\bar{D}^{*0}$ threshold when x is small and moves to it when $x \approx 1$. If x further increases this 1st sheet pole acrosses the $D^0\bar{D}^{*0}$ brach cut point in the real axis to the 2nd Riemann sheet and goes away(the trajectory of this pole is marked with red empty circles in Figs. 4(a) and 4(b)). It then moves again far away from the region we are studying if we keep increasing x. The other pair of poles on the 1st and 2nd sheets (black cross circle and full blue circle) move just a few MeV when we vary x.

The main effect of bubble chain in Fit III is to bring a new narrow resonance pole below the $D^0\bar{D}^{*0}$ threshold and cause a sharp spike in the $J/\Psi\pi\pi$ decay spectrum (it could not be seen in $D\bar{D}^*$ decays). We hope that data with better energy resolution can eventually discern the presence or no of this additional narrow resonance pole.

IV. CONCLUSION

In this article we explored the nature of the $X(3872)$ through an effective Lagrangian model to describe the energy region around the $D\bar{D}^*$ thresholds. The decays $B^+ \to K^+ D^0 \bar{D}^{*0}$ and $B^+ \to K^+ J/\psi\pi^+\pi^-$ were analyzed. We investigated whether the $X(3872)$ resonance is mainly an elementary particle, a $D\bar{D}^*$ molecule or and admixture of both. In the analysis where it is assumed to be a pure $c\bar{c}$ state with no $D\bar{D}^*$ component (Fit I), the DD^*DD^* four particles coupling constant λ_2 is set to zero. The $D\bar{D}^*$ rescatterings through an intermediate s–channel $X(3872)$ propagator reproduces the line-shape of the spectrum rather well, indicating that the X(3872) is mainly a standard Breit-Wigner resonance. In the pure molecule analysis (Fit II), the couplings of the elementary $X(3872)$ with other particles were set to zero (g_1, g_2, $g_4 = 0$ in Eq. (22)) and, alternatively, the coupling constant λ_2 played the crucial role in the B decays. In this case, the $D\bar{D}^*$ contact final state interaction (ruled by λ_2) determined the spectrum line-shape. We studied also the mixed scenario (Fit III), with the $X(3872)$ containing both elementary $c\bar{c}$ and $D\bar{D}^*$ molecular components which interact with each other in the B decay. However, the $D\bar{D}^*$ loops from the direct $D\bar{D}^* \to D\bar{D}^*$ contact interaction may have some non-negligible effects which needs further analysis. Meanwhile, Fit III was found to be unstable with the available data and no definitive conclusion could be extracted. Therefore our fits tend to favor a mostly elementary $X(3872)$.

For Fit II (only bubble chains with contact $D\bar{D}^*$ rescattering), we only find a pole in the 2nd Riemann sheet, corresponding to a virtual state. In the favored scenario Fit I, the lighter channels accounted through $\Gamma_{J/\psi\pi\pi}$, $\Gamma_{J/\psi\pi\pi\pi}$ and Γ_0 play an important role for the $X(3872)$ pole position, being $D\bar{D}^*$ contributions subdominant.

Our optimal scenario (Fit I) yields the 1st Riemann sheet pole determination (extracted from the fit parameters through a Monte Carlo simulation)

$$M^{1st}_{X(3872)} \;=\; (\, 3871.2 \pm 0.7 \,)\,\text{MeV}\,, \qquad \Gamma^{1st}_{X(3872)} \;=\; (\, 6.5 \pm 1.2 \,)\,\text{MeV}\,. \tag{26}$$

This narrow state is very near to the $D^0\bar{D}^{*0}$ threshold ($M_{D^0} + M_{\bar{D}^{*0}} = 3871.3$ MeV). Going over the $D^0\bar{D}^{0\,*}$ branch cut point one has access to the 2nd Riemann sheet, where we find a pole with position

$$M^{2nd}_{X(3872)} \;=\; (\, 3870.5 \pm 0.2 \,)\,\text{MeV}\,, \qquad \Gamma^{2nd}_{X(3872)} \;=\; (\, 7.9 \pm 1.6 \,)\,\text{MeV}\,. \tag{27}$$

This pole is again located in the complex plane in the neighborhood of the $D^0 \bar{D}^{*0}$ threshold. The widths of these 1st and 2nd sheet poles are consistent with the broad structure observed in Fig. 3, with a width in the spectrum of the order of 5-10 MeV.

Acknowledgments

Appendix A: The supression of longitudinal part near threshold

In Sec. II, the longitudinal part was argued to be a small quantity compared to the transverse part. Here we provide the proof. Since for physical on-shell polarization $p_{D^*} \cdot \epsilon_{D^*} = 0$, we have that $p \cdot \epsilon_{D^*} = p_D \cdot \epsilon_{D^*}$, with $p = p_D + p_{D^*}$. In the $D\bar{D}^*$ rest-frame one finds

$$
\begin{aligned}
p^\mu_{D^*} - \frac{p^\mu}{2} &= (\frac{\sqrt{m^2_{D^*} + |\vec{p}_{D^*}|^2} - \sqrt{m^2_D + |\vec{p}_{D^*}|^2}}{2}, \vec{p}_{D^*}) \\
&= (\frac{\Delta_m}{2}(1 - \frac{|\vec{p}_{D^*}|^2}{m_D m_{D^*}}), \vec{p}_{D^*}) \\
&\approx (\frac{\Delta_m}{2}, \vec{p}_{D^*}),
\end{aligned}
\tag{A1}
$$

where $\vec{p}_{D^*}$ is three momentum of p_{D^*} and $\Delta_m = m_{D^*} - m_D$. All the Lorentz components of $(p^\mu_{D^*} - p^\mu/2)$ are very small near the $D\bar{D}^*$ threshold. One can see in Eq. (11) that the transverse part is proportional to $p_K \cdot \epsilon_{D^*}$ while the longitudinal component carries a factor $p \cdot \epsilon_{D^*} = (p - 2p_{D^*})\epsilon_{D^*}$, which is small near the $D\bar{D}^*$ threshold. Another reason for the tiny longitudinal part is that there is no pole in the longitudinal part of the propagator in the energy region we are studying (close to the $D\bar{D}^*$ threshold) and the corresponding denominator does not enhance the amplitude as it occurs with the transverse component.

Appendix B: The loop integrals

In Sec. II, we make use of the Feynman integral

$$
\int \frac{d^D k}{(2\pi)^D} \frac{g_{\mu\nu} - \frac{k_\mu k_\nu}{m^2_{D^{*0}}}}{(k^2 - m^2_{D^{*0}} + i\epsilon)((p-k)^2 - m^2_{D^0} + i\epsilon)} = P_{T\mu\nu}\Pi_{T_{D^0\bar{D}^{*0}}} + P_{L\mu\nu}\Pi_{L_{D^0\bar{D}^{*0}}},
\tag{B1}
$$

where $\Pi_{T_{D^0\bar{D}^{*0}}}$ and $\Pi_{L_{D^0\bar{D}^{*0}}}$ are

$$
\begin{aligned}
\Pi_{T_{D^0\bar{D}^{*0}}}(P^2) &= \frac{-i}{16\pi^2}(\frac{1}{2}I_0 - \frac{p^2}{2m^2_{D^*}}I_2 + \frac{p^2 + m^2_{D^*} - m^2_D}{2m^2_{D^*}}I_1 - \frac{\frac{1}{3}p^2 - (m^2_{D^*} + m^2_D)}{4m^2_{D^*}}) \\
&\quad - \frac{iR}{16\pi^2}(1 + \frac{p^2}{12m^2_{D^*}} - \frac{m^2_{D^*} + m^2_D}{4m^2_{D^*}}), \\
\Pi_{L_{D^0\bar{D}^{*0}}}(p^2) &= \Pi_{T_{D^0\bar{D}^{*0}}}(p^2) + \frac{i}{16\pi^2}\frac{p^2}{m^2_{D^*}}I_2 + \frac{iR}{16\pi^2}\frac{p^2}{3m^2_{D^*}},
\end{aligned}
\tag{B2}
$$

with the ultraviolet divergence $R = -\frac{1}{\epsilon} + \gamma_E - ln4\pi$ and $\epsilon = \frac{4-D}{2}$.

The values for the I_n integrals are

$$
I_n = \int_0^1 x^n ln\frac{m^2_D x + m^2_{D^*}(1-x) - p^2 x(1-x)}{\mu^2}dx,
\tag{B3}
$$

$$I_0 = -B_0(s),$$

$$I_1 = -\frac{1}{2}(1 + \frac{m_{D*}^2 - m_D^2}{s})B_0(s) + \frac{1}{2s}(A_{D*} - A_D),$$

$$I_2 = -\frac{1}{3}[(1 + \frac{m_{D*}^2 - m_D^2}{s})^2 - \frac{m_{D*}^2}{s}]B_0(s) + \frac{1}{3s}(A_{D*} - 2A_D)$$
$$-\frac{1}{18} + \frac{m_{D*}^2 - m_D^2}{3s^2}(A_{D*} - A_D) + \frac{1}{6s}(m_{D*}^2 + m_D^2). \quad (B4)$$

The A and B functions are:

$$A_{D*} = -m_{D*}^2(-1 + ln\frac{m_{D*}}{\mu^2}),$$

$$A_D = -m_D^2(-1 + ln\frac{m_D}{\mu^2}),$$

$$B_0(s) = 2 - ln\frac{m_D^2}{\mu^2} + \frac{s + m_{D*}^2 - m_D^2}{2s}ln\frac{m_D^2}{m_{D*}^2} + \rho(s)ln\frac{\lambda(s) - 1}{\lambda(s) + 1}, \quad (B5)$$

with $\rho(s) = \frac{\sqrt{(s-(m_D+m_{D*})^2)(s-(m_D-m_{D*})^2)}}{s}$ and $\lambda(s) = \sqrt{\frac{s-(m_D+m_{D*})^2}{s-(m_D-m_{D*})^2}}$. In the 1st Riemann sheet we have $\rho(s+i\epsilon) = |\rho(s)|$ over threshold and $\rho(s) = i|\rho(s)|$ below.

We renormalize the amplitude through the threshold substraction,

$$\hat{\Pi}_{T_{D^0\bar{D}^{*0}}}(s) = \Pi_{T_{D^0\bar{D}^{*0}}}(s) - \Pi_{T_{D^0\bar{D}^{*0}}}(s_{th}),$$

$$\hat{\Pi}_{L_{D^0\bar{D}^{*0}}}(s) = \Pi_{L_{D^0\bar{D}^{*0}}}(s) - \Pi_{L_{D^0\bar{D}^{*0}}}(s_{th}), \quad (B6)$$

where $s_{th} = 3871.3$MeV is the threshold of $D^0\bar{D}^{*0}$ channel. Near this threshold the self-energy shows the behaviour

$$\hat{\Pi}_{T_{D^0\bar{D}^{*0}}}(s) = \frac{1}{16\pi}(-\rho(s) + O(\rho^2(s)),$$

$$\hat{\Pi}_{L_{D^0\bar{D}^{*0}}}(s) = \frac{1}{16\pi}(\rho^3(s) + O(\rho^4(s)). \quad (B7)$$

For the charged channel we use threshold subtraction with $s_{th} = 3879.4$MeV.

[1] S.-K. Choi et al. (Belle Collaboration), Phys. Rev. Lett. 91, 262001 (2003).
[2] D. Acosta et al. (CDF Collaboration), Phys. Rev. Lett. 93, 072001 (2004).
[3] V. M. Abazov et al. (D0 Collaboration), Phys. Rev. Lett. 93, 162002 (2004).
[4] B. Aubert et al. (BaBar Collaboration), Phys. Rev. D 71, 071103 (2005).
[5] R. Aaij et al. (LHCb Collaboration), Eur Phys. J.C 72, 1972 (2012).
[6] V. Chiochia et al. (CMS Collaboration), arXiv:hep-ex/1201.6677.
[7] S.-K. Choi et al. (Belle Collaboration), Phys. Rev. D 84, 052004 (2011).
[8] R. Aaij et al. (LHCb Collaboration), Phys. Rev. Lett. 110, 222001 (2013).
[9] Qing Gao et al. (BESIII Collaboratbion), Int.J.Mod.Phys.Conf.Ser. 31, 1460307(2014).
[10] B. Aubert et al. (BaBar Collaboration), Phys. Rev. D 73, 011101 (2006).
[11] B. Aubert et al. (BaBar Collaboration), Phys. Rev. D 77, 111101 (2008).
[12] I. Adachi et al. (Belle Collaboration), arXiv:0809.1224.
[13] B. Aubert et al. (BaBar Collaboration), Phys. Rev. D 77, 011102(2008).
[14] T. Aushev et al. (Belle Collaboration), Phys. Rev. D 81, 031103(R)(2010).
[15] K. Abe et al. (Belle Collaboration), hep-ex/0505037.
[16] B. Aubert et al. (BABAR Collaboration), Phys. Rev. Lett. 102, 132001(2009).
[17] R. Aaij et al. (LHCb Collaboration), Nucl. Phys. B 886, 665 (2014).
[18] K.A. Olive et al. (Particle Data Group), Chin. Phys. C, 38, 090001 (2014).
[19] C. Meng, K. T. Chao, Phys. Rev. D 75, 114002(2007).
[20] P. Wang, X. G. Wang, Phys. Rev. Lett 11, 042002(2013).
[21] C. E. Thomas and F. E. Close, Phys. Rev. D 78, 034007(2008).
[22] E. Braaten, H. W. Hammer, Thomas Mehen, Phys. Rev. D 82, 034018(2010).
[23] V. Baru et al, Physics Letters B 726, 537(2013).
[24] C. Hanhart, Yu. S. Kalashnikova, A. E. Kudryavtsev and A. V. Nefediev, Phys. Rev. D76, 034007 (2007).
[25] L. Maiani et al. Phys. Rev. D 71, 014028(2005).
[26] W. Chen, Phys. Rev. D 88, 045027(2013).
[27] C. Meng, Y. J. Gao and K. T. Chao, Phys. Rev. D 87, 074035 (2013) [hep-ph/0506222].

[28] M. Suzuki, Phys. Rev. D 72, 114013(2005) [hep-ph/0508258].

[29] B. Q. Li, C. Meng and K. T. Chao, Phys. Rev. D 80, 014012 (2009).

[30] I. V. Danilkin, Yu. A. Simonov, Phys. Rev. Lett. 105, 102002 (2010).

[31] Yu. S. Kalashnikova and A. V. Nefediev, Phys. Rev. D 80, 074004 (2009).

[32] C. Meng, H. Han, K.T. Chao, arXiv:1304.6710 [hep-ph].

[33] Ou Zhang, C. Meng and H. Q. Zheng, Phys.Lett. B 680, 453(2009).

[34] D. Morgan, Nucl. Phys. A543, 632(1992).
D. Morgan and M. R. Pennington, Phys. Rev. D48, 1185(1993).

[35] Guo-Ying Chen and Q. Zhao, Phys.Lett. B 718, 1369(2013).

[36] N. N. Achasov and A. A. Kozhevnikov, Phys. Rev. D 83, 113005(2011).

[37] M. T. AlFiky, F. Gabbiani and A. A. Petrov, Phys.Lett. B 640, 238(2006).

[38] E. Braaten, M. Kusunoki, Phys. Rev. D 69, 074005(2004) .

[39] S. Fleming, T. Mehen, AIP Conf. Proc. 1182, 491 (2009) [hep-ph/0907.4142].

[40] P. Artoisenet, E. Braaten and D. Kang, Phys. Rev. D 82, 014013(2010).

[41] Notice the minus sign in the upper component of the doublet, as under isospin transformations $\begin{pmatrix} u \\ d \end{pmatrix} \longrightarrow S \begin{pmatrix} u \\ d \end{pmatrix}$ one has the conjugate doublet $\begin{pmatrix} -\bar{d} \\ \bar{u} \end{pmatrix}$ transforming like $\begin{pmatrix} -\bar{d} \\ \bar{u} \end{pmatrix} \longrightarrow S \begin{pmatrix} -\bar{d} \\ \bar{u} \end{pmatrix}$. In our D mesons we have the quark content $D^+ \sim c\bar{d}$ and $D^0 \sim c\bar{u}$, which gives the isodoublet D in the text [40]. The hermitian conjugate of the isodoublet transforms with S^{-1} acting from the right and can be used to build isospin invariant operators.

[42] E. Braaten, J. Stapleton, Phys. Rev. D 81, 014019(2010).

[43] L. Y. Dai, X. G. Wang, H. Q. Zheng, 2012 Commun. Theor. Phys. 57 841.